Accepted Manuscript

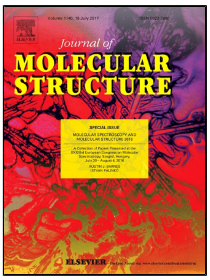

Quantum, characterization and spectroscopic studies on Cu(II), Pd(II) and Pt(II) complexes of 1-(benzo[*d*]thiazol-2-yl)-3-phenylthiourea and its biological application as antimicrobial and antioxidan

Suhair M. S. Jamb

PII:	S0022-2860(17)30507-0
DOI:	10.1016/j.molstruc.2017.04.065
Reference:	MOLSTR 23688
To appear in:	*Journal of Molecular Structure*
Received Date:	24 January 2017
Revised Date:	15 April 2017
Accepted Date:	17 April 2017

Please cite this article as: Suhair M. S. Jamb, Quantum, characterization and spectroscopic studies on Cu(II), Pd(II) and Pt(II) complexes of 1-(benzo[*d*]thiazol-2-yl)-3-phenylthiourea and its biological application as antimicrobial and antioxidan, *Journal of Molecular Structure* (2017), doi: 10.1016/j.molstruc.2017.04.065

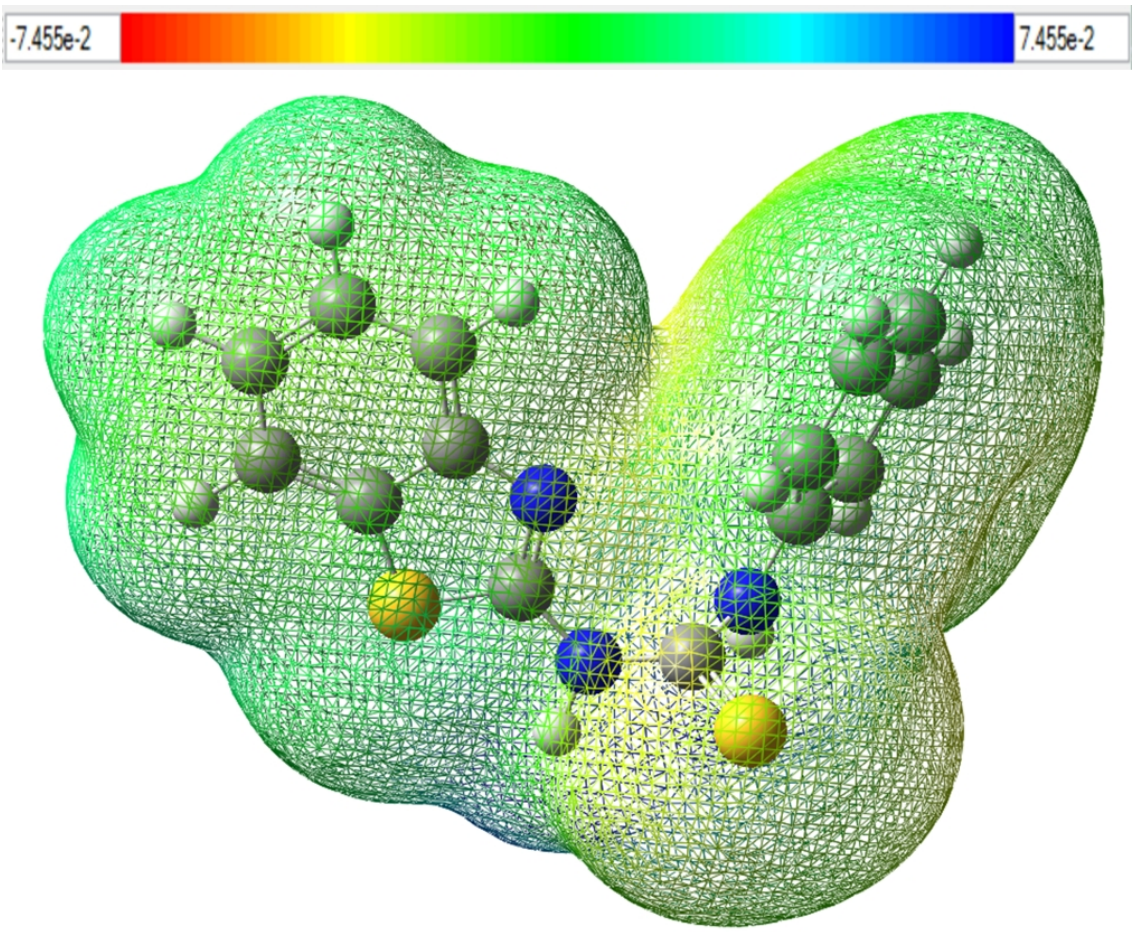

Molecular electrostatic potential map for H_2PhT.

- Preparation of Cu^{2+}, Pd^{2+} and Pt^{2+} complexes of phenylthiourea derivatives.
- Elemental analysis, magnetic susceptibilities and spectroscopic estimations of the ligand and its complexes.
- Molecular modeling, chemical reactivity, MEP, NLO, Mulliken atomic charges, and binding energy were estimated for the investigated compounds.
- Theoretical infrared intensities and ^{1}H NMR of the ligand was computed utilizing DFT technique.
- DNA bioassay, antibacterial and antifungal activities of the compounds have been determined.

Quantum, characterization and spectroscopic studies on Cu(II), Pd(II) and Pt(II) complexes of 1-(benzo[*d*]thiazol-2-yl)-3-phenylthiourea and its biological application as antimicrobial and antioxidant

Abstract

Divalent platinum, palladium and copper chelates of H_2PhT have been isolated and identified. Their structures have been elucidated by partial elemental analyses, magnetic susceptibilities and spectroscopic estimations and additionally mass spectra. The FTIR and ^1H NMR studies illustrated that H_2PhT performs as mono-negative bi-dentate in Cu(II) and Pd(II) complexes while it behaves as neutral bi-dentate in both Pt(II) complexes. Both magnetic moments and spectral studies suggests a tetrahedral coordination geometry for $[Cu(HPhT)(H_2O)Cl]$ complex, a square planar geometry for both $[Pd(HPhT)_2]$ and $[Pt(H_2PhT)_2Cl_2]$ complexes and octahedral geometry for $[Pt(H_2PhT)_2Cl_2]$ complex. The molecular modeling are drawn and demonstrated both bond lengths and angles, chemical reactivity, MEP, NLO, Mulliken atomic charges, and binding energy (kcal/mol) for the investigated compounds. Theoretical infrared intensities and ^1H NMR of H_2PhT was computed utilizing DFT technique. An examination of the experimental and hypothetical spectra can be extremely valuable in making right assignments and analyzing the main chemical shift. DNA bioassay, antibacterial and antifungal activities of the investigated compounds have been determined.

Key words: Thiazole, thiourea, DFT, NLO, theoretical IR, DNA bioassay and antimicrobial studies.

1. Introduction

Thioureas containing thiazole ring and their chelates have found wide applications in exceptional pharmacological items as penicillin and vitamins. They can bind DNA, RNA, in addition to their anti-diabetic, anti-cancer, anti-viral, anti-microbial and anti-fungal properties. Also, literature survey of thioureas transition metal chelates, particularly platinum chelates illustrated interesting applications in anticancer medications. As a ligand, the thiazole moiety is conceivably ambidentate and can coordinate the metal ions either through the thione or thiol forms. The ability of thiazoles to coordinate to Cu^{2+}, Pd^{2+} and Pt^{2+}, soft acids, indicated coordination to the marginal base azomethine nitrogen atom and thiazole sulfur atom [1-4]. With regards to the

above applications, we have reported here the synthesis and spectroscopic studies on the ligand (H_2PhT) and its Cu(II) , Pt(II) and Pd(II) chelates. The proposed structures were supported by geometry optimization of the ligand and its chelates.

2. Experimental

2.1. Materials and Instruments

The following compounds were bought from Sigma Aldrich and utilized as received. The elemental analyses were done on Research Center, College of Pharmacy, and KSU Riyadh using "a Perkin–Elmer elemental instrument". Standard techniques was utilized to estimate the contents of metal and chloride in the chelates [5]. Estimation of the molar conductance for the chelates in DMF was estimated utilizing "a Tacussel bridge (CD6NG)".^{1}H- and ^{13}C NMR were obtained with a JEOL 400 MHz NMR spectrometer, in deuterated dimethylsulfoxide (DMSO-d_6) at room temperature utilizing tetramethylsilane (TMS) as an internal standard. D_2O-exchange was utilized to affirm the identification of the NH- signals. Fourier transform infrared (FTIR) spectra were recorded using a Bruker Tensor 27 FTIR spectrophotometer (Bruker Optics GmbH, Ettlingen, Germany) utilizing KBr pellets. Unicam UV–Vis spectrophotometer were utilized to record UV–Vis. spectra. The estimation of magnetic moment was done on a "Sherwood magnetic balance" at 25 ^{o}C. EI-MS were measured on Finnigan 711A (8 kV) and recorded as $\frac{mass}{charge}(\frac{m}{z})$.

2.2. Preparation of 1-(benzo[*d*]thiazol-2-yl)-3-phenylthiourea (H_2PhT)

By mixing 1:1 molar ratio of 2-aminobenzothiazole (1.50 g, 0.01mol) and phenyl isothiocyanate (1.35 g, 0.01mol) in 30 ml hot ethanolic solution. The reaction mixture was refluxed for 3.5 hrs. Pale yellow precipitate was separated after cooling, then isolated, recrystallized by hot C_2H_5OH and lastly desiccated over P_2O_5. The purity was checked by TLC. $C_{14}H_{11}N_3S_2$ (285.38). % Found (Calcd.): C 58.62 (58.92), H 3.65 (3.89), N 14.64 (14.72). Mass spectrum: *m/z* = 285 (63%) corresponding to ($C_{14}H_{11}N_3S_2$).

2.3. Synthesis of metal complexes

[Cu(HPhT)(H_2O)Cl], [Pd(HPhT)$_2$] and [Pt(H_2PhT)Cl_2] chelates were synthesized by refluxing H_2PhT (0.285 g, 1.0 mmol) and 1.0 mmol of metal salt; 0.17 g of $CuCl_2.2H_2O$, 0.22 g of $Pd(CH_3COO)_2$ or 0.42 g of K_2PtCl_4 in 20 ml ethanol for 6 h. On the other hand, [Pt(H_2PhT)$_2Cl_2$] was prepared by using 2.0 mmol of H_2PhT ligand with 1 mmol of K_2PtCl_4. The produced hot chelates were separated, washed with C_2H_5OH then $C_2H_5OC_2H_5$ and desiccated over P_2O_5.

2.4. Quantum chemical computations

The main errand for the theoretical studies is to decide the most stable geometry of H_2PhT and its metal chelates. Computational DFT were performed for H_2PhT by (B3LYP) function together utilizing "6-311++G(d,p)" basis set while semi-empirical method was utilized for the complexes to infer the entire geometry stabilization and ordinary-style examination for separated chelates [6-8]. Lorentzian band shapes with full width at half maximum was utilized to sketch the calculated IR spectrum. The improved structure was utilized to register the minimal spin-permitted electronic vertical excitation energies utilizing (B3LYP) with standard Pople basis set that incorporates diffuse functions on atoms (6-311 ++ G (d, p). The electronic properties, for example frontier molecular orbitals, dipole moments and infrared intensities were ascertained.

Computations on proton magnetic shielding values were done utilizing (GIAO) approach [9, 10] for gas phase. This methodology permits the calculation of the indisputably chemical shielding because of the electronic surroundings of the respective cores. The chemical shift was estimated hypothetically by using the exact level of speculation on TMS. DFT studies have been utilized to ascertain the dipole moment, mean polarizability and first static hyperpolarizability into account the constrained field ideology. The basic and spectroscopic portrayal of a unfaltering molecule was done utilizing Gaussian 09 program bundle on the private PC [11].

2.5. DNA-methyl green bioassay [12, 13]

100 ml of 0.05 M Tris-HCl buffer (pH 7.5) containing 7.5 mM $MgSO_4$ was added to 20 mg of DNA methyl green; the mixture was disintegrated at 310 K for 24 h. Test samples 10,100, 1000 mg) were dissolved in ethanol in Ependoff tubes. After that, the solvent was evacuated under vacuum, then a solution containing 200µl of the DNA/methyl green was poured into each separate Ependoff. Samples were hatched at surrounding temperature. Beyond one day, the absorbance of the samples was evaluated at 645 nm. Readings were adjusted for starting absorbance and standardized as the rate of the unstained standard.

2.6. Antimicrobial and antimycotic activities in terms of MIC (µg/mL) [14]

The anti-bacterial behavior of H_2PhT and its divalent Cu, Pd and Pt chelates was investigated against strains disengaged from animal by-products and were blamed for being immediate reason of nourishment inebriation in human. The strains incorporate *Staphylococcus aureus* "Gram-positive bacteria" and *Escherichia coli* "Gram-negative bacteria" utilization Muller

Hinton agar medium. The anti-fungal behavior of the materials were studied against *(Candida albicans)* using Sabouraud dextrose agar medium (Oxoid). Ciprofloxacin (100 µg/ml) and Fluconazole (100 µg/ml) were utilized as standard for hostile to bacterial and against parasitic movement.

Agar steak dilution method was utilized to determine MIC of the investigated compounds. 100 µg/ml stock solution of the studied compound in DMSO and measured amounts of the studied materials were consolidated in a determined amount of molten sterile agar (Muller Hinton agar for anti-microbial studies and "Sabouraud dextrose agar" one for anti-parasitic action). A pre-determined amount of this medium at 50 °C containing the material was poured into a Petri dish to yield a profundity of 4 mm and permitted to densify. 105 cfs/ml of a suspension of the micro-organism was applied to plates with serially diluted compounds in DMSO to be checked and incubated at 37 °C for one and two days for microbes and parasites, individually. The MIC is the least amount of the investigated material showing no unmistakable development of microorganisms or organisms on the plate.

3. Results and discussion

Table 1 outlines the data of elemental analysis and some physical properties of the chelates. The stoichiometries of the coordination adducts set up by elemental analysis are affirmed by geometry optimization. The non-electrolytic nature of the chelates was assessed by the small quantity of molar conductivity (1.0 – 17.0 cm^2 ohm^{-1} mol^{-1}) [15]. Disappointingly, single crystals of the investigated chelates cannot be obtained. The purity of the H_2PhT ligand was examined by TLC (silica gel). The chelates were non-hygroscopic and insoluble in typical organic solvents but soluble in DMSO. All the chelates showed melting point above 300 ºC.

3.1. IR spectra

The IR spectrum of H_2PhT and its divalent chelates were performed as KBr disc in the 4000-400 cm^{-1} scope. Table 2 demonstrates the FTIR spectra of H_2PhT and its chelates. The IR spectrum of H_2PhT displays bands at 3436, 3162 and 804 cm^{-1}, attributable to $\upsilon(N^1–H)$, $\upsilon(N^2\text{-}H)$ and υ(C=S), individually. There are no bands in the 2290-2495 cm^{-1} range attributable to υ(S-H) which confirms the existence of H_2PhT in the thione form in the solid state (Structure 1a). The bands at 1569 and 1528 cm^{-1} due to ν(C=C) and ν(C=N) of the thiazole ring vibrations, consequently. In both Cu and Pd complexes (Structures 2, 3), H_2PhT acts as a mono-negative bi-

dentate ligand attached to the nitrogen atom of the thiazole moiety and the C=S group in the thiol isomer. This behavior is illustrated by (i) the absence of $\upsilon(N^1–H)$, (ii) the movement of $\nu(C=N)_{Py}$ frequeny. (iii) the shift of ν(C=S) peaks to lower wavenumbers with the appearance of new bands at 1535, 1527, 1156 and 1132 due to ν(N=C-S) and ν(C-S), respectively. In both platinum chelates (Structures 4, 5), H_2PhT behaves as a neutral bi-dentate attached to the nitrogen atom of the thiazole moiety and the C=S group of the thione form. This behavior is confirmed by (i) the shift of $\upsilon(N^1–H)$ to large wavenumber. (ii) the shift of ν(CS) to lower wavenumber, proposing the coordination to Pt(II) by the thione-Sulfur atom while the $\upsilon(N^2–H)$ band moved to higher wavenumbers.

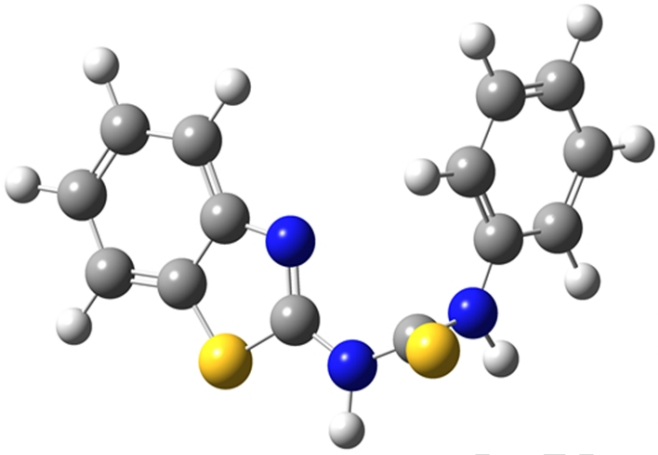

Structure 1a. Molecular modeling of H_2PhT in the thione form.

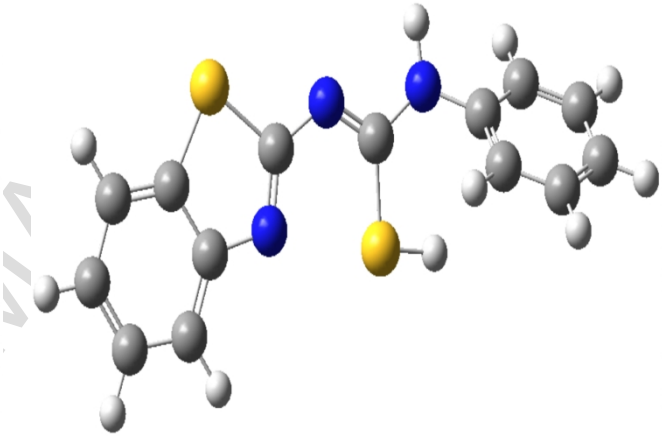

Structure 1b. Molecular modeling of H_2PhT in the thiol form.

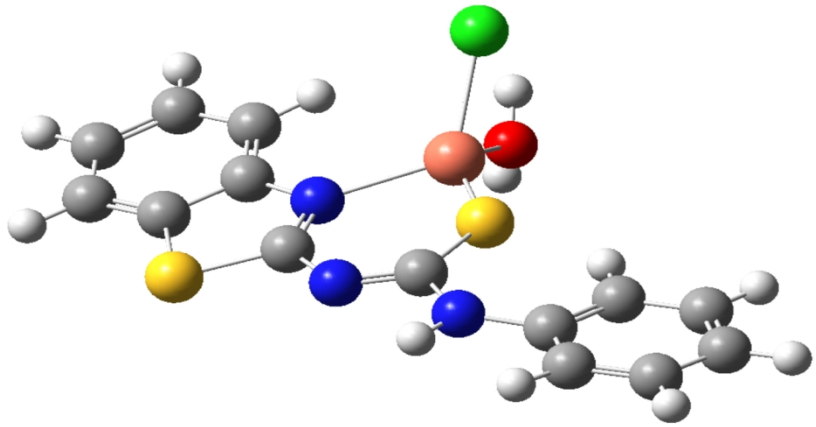

Structure 2. Molecular modeling of [Cu(HPhT)(H_2O)Cl].

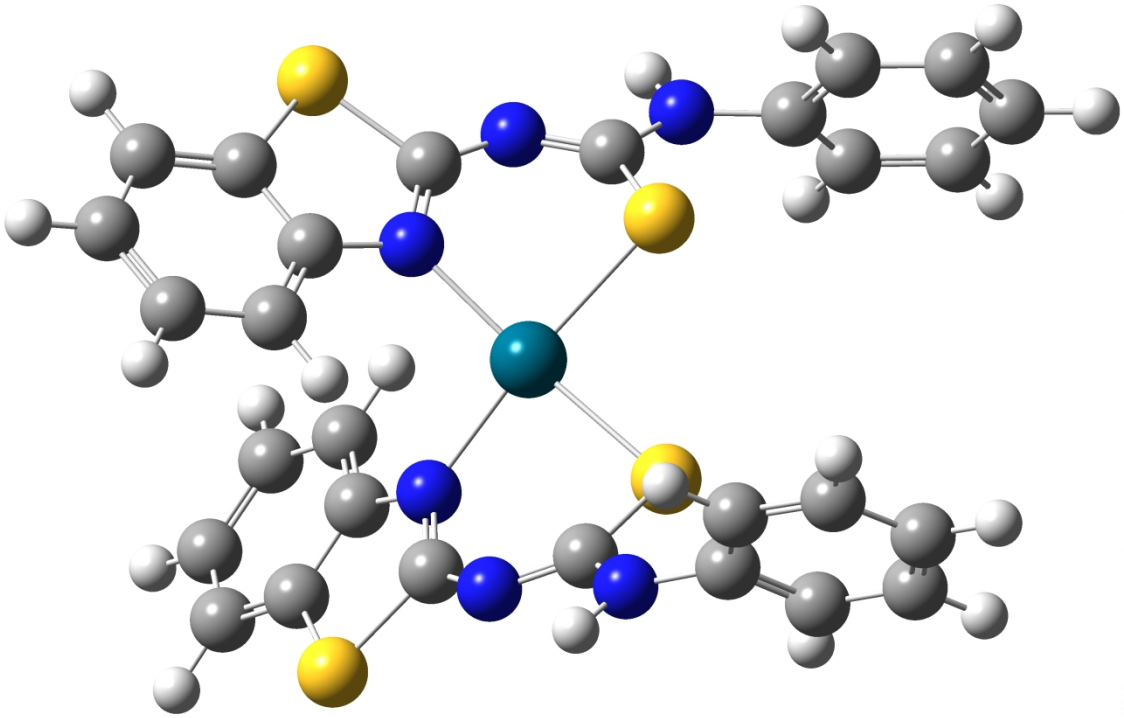

Structure 3. Molecular modeling of [Pd(HPhT)$_2$].

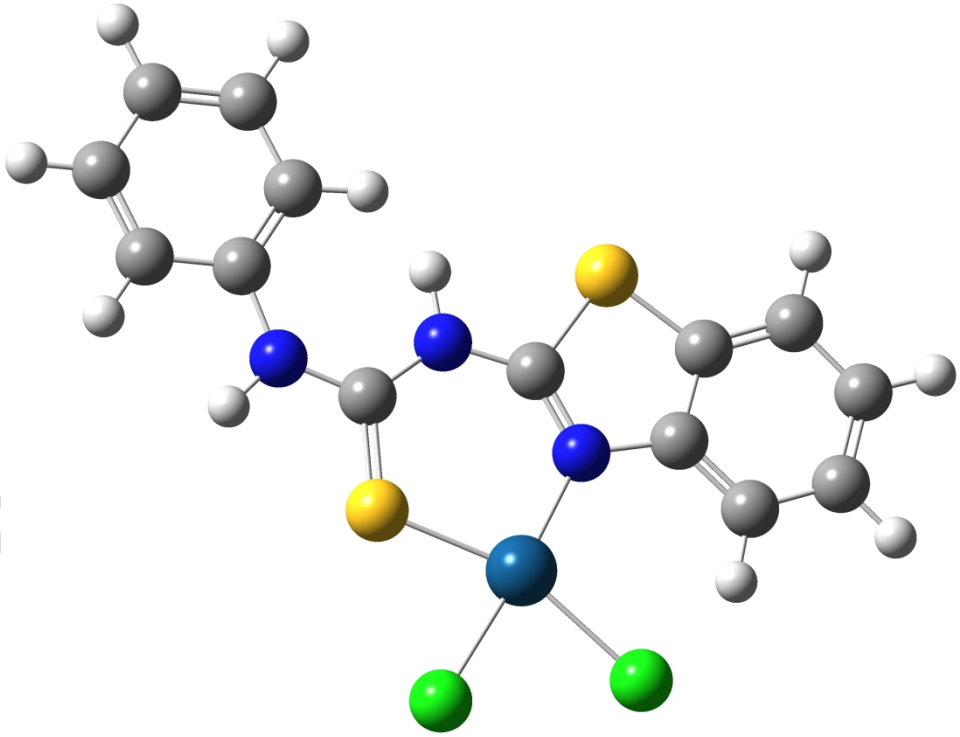

Structure 4. Molecular modeling of [Pt(H_2PhT)Cl_2].

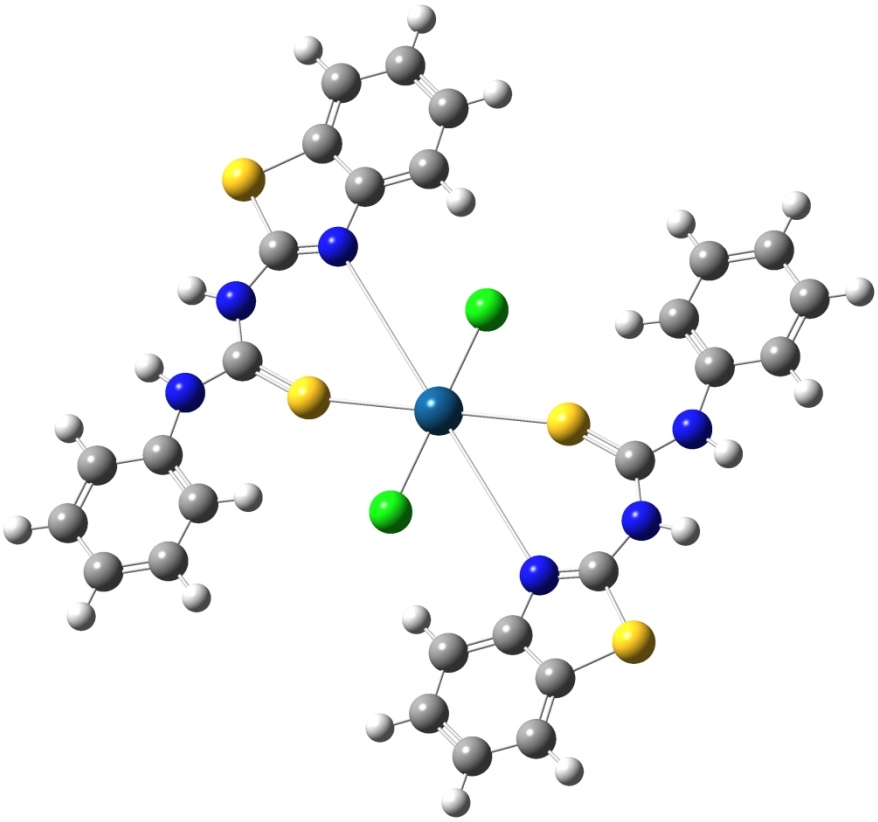

Structure 5. Molecular modeling of [Pt(H_2PhT)$_2Cl_2$].

3.2. ^{1}H NMR spectra

The ^{1}H NMR spectrum of the H_2PhT in DMSO-d_6 illustrates the existence of the ligand in the thiol form in solution (Structure 1) under the test settings. The presence of signals at 1.92 and 10.46 ppm assignable to (SH) and (NH) protons, respectively. The signals of all aromatic hydrogen are in the range of (7.28 – 7.95 ppm) equivalent to 10 protons of the thiol tautomer. In case of both platinum chelates, the signal at 10.46 ppm assignable to (NH) protons in the ^{1}H NMR spectrum of the ligand still exist in the ^{1}H NMR spectrum of these complexes but shifted to downfield confirming the neutrality of the ligand and the coordination via both C=S and C=N groups while the signal at 1.92 ppm due to (SH) proton disappears. Further evidence for deprotonation of the thiol group in [Pd(HPhT)$_2$] comes from the ^{1}H NMR spectrum, asserting the weakness of the signals of the (NH) protons while the signal at 1.92 ppm due to SH proton disappears.

3.3. ^{13}C-NMR spectra

The ^{13}C-NMR spectra of H_2PhT and its divalent chelates in DMSO-d_6 illustrated signals assignable to carbon atoms in the phenyl, thiazole and C=S groups. The following points can be

illustrated by comparing the chemical shift values of the chelates with those of H_2PhT: (i) An upfield move for the (CS) carbon from 172.00 ppm in the H_2PhT to 170.84 ppm in $[Pd(HPhT)_2]$ containing the mono-anion ligand. This is due to the complexation of the S atom to Pd^{II} metal. (ii) An upfield move for the (C=S) carbon from 172.00 ppm in H_2PhT to 171.06-169.08 ppm in both Pt^{II} chelates containing the neutral ligand. (iii) No obvious pattern was noticed in the shift of signals of aromatic ring carbons. The previous behavior might be credited to the contradicting impact of σ-electron withdrawing and π-bonding donation over those carbons that are affected by the coordinated metals [16, 17].

3.4. Electronic spectra and magnetic behavior

All chelates are diamagnetic at 300 K, with the exception of Cu(II) one which has paramagnetic property (μ_{eff} = 1.93 B.M./Cu atom). This indicate a tetrahedral arrangement around divalent palladium and platinum chelates. The electronic spectra of the ligand and its chelates were displayed in Nujol mull. The spectrum of the H_2PhT ligand shows an intense absorption band at 261 nm assignable to $\pi \rightarrow \pi^*$ transition of thiazole ring. Another intense band is seen at 298 nm (33557 cm^{-1}) attributable to $\pi \rightarrow \pi^*$ of (C=N) group which shifts in chelates to higher frequencies, proving the complexation of H_2PhT via $(C=N)_{azomethine}$ nitrogen atom. The band at 361 nm attributable to $(n \rightarrow \pi^*)_{thiazole}$, transitions. Electronic spectra of copper complex can be an indicator of its geometry [18]. The electronic spectrum of Cu complex shows an absorption band in the region of 370 nm indicating a four-coordinated geometry of Cu(II) [18, 19]. The band at 273 nm might be attributable to intra-ligand charge transfer (CT) transitions.

The coordination and the kind of the metal affects this band as illustrated by marginally shorter wavelengths moves with splitting in both divalent Pt and Pd chelates. This might be credited to the broad delocalization of π system by the clear π-back coordination M→L between Pt^{2+} and Pd^{2+} ions and both CS and CN atoms. The new band showed up at 316 and 341 nm in Pt(II) chelates.

The d-d bands from the spectra of the Pd chelate having low intensities appeared at 461 nm and were assigned to the $^1A_{1g} \rightarrow {}^1A_{2g}$ transition in square planar environment around palladium [16, 20]. Other bands from the spectra of the complex are too intense to be assigned to d-d transition.

3.5. Molecular modeling

3.5.1. IR

Frequency estimation were done to earn the spectroscopic mark of H_2PhT. There are little contrasts amongst hypothetical and exploratory vibrational wavenumbers as appeared in Fig. 1. The main reason for this difference is that the calculation were done for uncoordinated H_2PhT in vacuum, yet the examinations were accomplished for solid H_2PhT. The vibrational modes of H_2PhT are exceptionally complex because of its low symmetry. Particularly, torsion, in- and out-of plane modes are hard to allocate as a result of interpreting with the ring modes furthermore with the derivative. In any case, there are some clear frequencies helpful to describe in the obtained chart. The correlation graphic portrayed concordance between the hypothetical and experimental wavenumbers (Fig. 2). There is linear relationship between the hypothetical and experimental wavenumbers as depicted by the next equation:

v_{cal} =0.98683v_{exp} + 18.5772 with correlation coefficients (R^2 = 0.99985).

3.5.2. ^{1}H NMR

The structure of bulky compounds can be investigated by combined utilization of experimental and computational tools. The obtained structure of H_2PhT after optimization is utilized to figure the ^{1}H NMR spectrum at B3LYP strategy with 6-311++G(d,p) level utilizing the GIAO method and the chemical shifts of H_2PhT are accounted for in ppm in respect to TMS for ^{1}H NMR which are introduced in Table 3. Theoretical ^{1}H NMR has a signal at 10.71 ppm attributable to only one NH proton confirming the presence of H_2PhT in the thiol form in a solution.

3.5.3. Chemical reactivity

3.5.3.1. Global reactivity descriptors

The assurance of energies of the HOMO and LUMO are essential criterion in quantum estimations. The HOMO “Highest Occupied Molecular Orbitals” is the one which principally behaves as an electron donor. On the other hand, the LUMO “Lowest Unoccupied Molecular Orbital” is the orbital that greatly behaves as the electron receiver. These orbitals are additionally named frontier molecular orbitals (FMOs).

i. The E_{HOMO} and E_{LUMO} and the adjoining levels are practically negative. This illustrate the stability of the isolated chelates [21-24].
ii. The FMOs hypothesis anticipate sites of electrophilic attack on aromatic ligands. The combination among these orbitals is an administering element in numerous responses. One has the ability to demonstrate that by the computation via scanning for the biggest estimations of

atomic orbital coefficients. Thus, orbitals of H_2PhT with the biggest quantity of coefficients might be treated as the places suitable for complexation. The previous outcome is affirmed by the information acquired from the computation since nitrogen of $(C=N)_{azomethine}$ and sulphur of $(C=S)_{thione}$ showed the biggest quantities.

iii. Gutmann's variation principle, ''the bond strength increases as the neighboring bonds get to be weaker'' which proved by Linert *et al*. [25]. This explanation agrees well with the results as the increase of the E_{HOMO} is accompanied by a weakness "elongation" of the M–L bonds. This promotes a fortifying "shortness" of the distances beside the M-L sites.

iv. The energy gap ($\Delta E = E_{HOMO} - E_{LUMO}$) is an a critical indicator that describes the chemical reactivity and kinetic stability for the investigated material [21]. H_2PhT is characterized by small energy showing that charge move fluently happens in it. The aforementioned factor affect the biological behavior of H_2PhT. The conjugation is the main reason for the small energy [26]. DFT strategy idea the substance reactivity and site selectivity of the atomic frameworks. E_{HOMO}, E_{LUMO}, ΔE which clarifies the inevitable charge exchange collaboration inside the studied material, electronegativity (χ), potential (μ), hardness (η), softness (S), electrophilicity (ω) and the softness (σ) [27, 28] are recorded in Table 4.

$$\chi = -1/2\ (E_{LUMO} + E_{HOMO}) \quad (1)$$

$$\mu = -\chi = 1/2\ (E_{LUMO} + E_{HOMO}) \quad (2)$$

$$\eta = 1/2\ (E_{LUMO} - E_{HOMO}) \quad (3)$$

$$S = 1/2\ \eta \quad (4)$$

$$\omega = \mu^2/2\ \eta \quad (5)$$

Electrophilicity record is a standout amongst the most critical quantum descriptors in depicting toxicity of various toxicity of different contaminations as far as their reactivity and site selectivity [29]. Likewise, the electrophilicity appropriately evaluates the biological behavior of medication receptor collaboration. This new reactivity record estimates the stabilization in energy when the framework obtains more electronic charge from the surrounding. The significance of η and σ is used to estimate both reactivity and stability.

3.5.4. Geometry optimization using DFT study

For the discussion of the optimized molecular structure. Examination of the information figured for the bond distances and angles, the following points can dedicated:

1. The HOMO level is largely localized on the N(7) and S(13) atoms (Fig. 3) showing that these atoms are the favored destinations for nucleophilic reaction at the central cation.
2. The counts demonstrated that the charge dispersion of the HOMO level of Cu-chelate is exceptionally confined on the lone pair of N and S atoms, and d-orbital of Cu^{II}- atom, (Fig. 4). The charge density of the LUMO level is, for the most part, distributed on the the nitrogen atoms and the phenyl group (Fig. 4).
3. While in Pd(II) chelate (Fig. 5), the charge distribution of the HOMO level is delocalized on the d-orbital of palladium and the lone pair of sulfur atom. On the other hand, the charge density of the HOMO level of Pd(II) and Pt(II) complexes is conveyed over the entire system.
4. Likewise, the charge of the LUMO level is exceedingly delocalized over the entire moiety of the chelate and on d-orbital of Pd and Pt metals (Figs. 5- 7). It was concluded from the above explanation that there is σ-donation from H_2PhT to the d-orbital of the metal together with back donation from the d-orbital of the metal atom to H_2PhT which enhances the stability of the examined chelates.

3.5.5. Molecular electrostatic potential (MEP)

The MEP is defined as a figure of electrostatic potential charted onto the stationary electron density surface. MEP is likewise extremely accommodating in research of the structure with its physio-chemical relationship and also hydrogen bonding collaborations [30-32]. This potential "V(r)" at any distance "r (x, y, z)" is characterized as far as the cooperation energy between the charge created by the proton, electrons and nuclei situated at this distance [33]. Calculation of this potential is feasible for particles utilizing the Γ-point and different k-focuses. In the recent paper, 3D graphs of "MEP" of H_2PhT and its metal chelates (Figs. 8-12) have been drawn. In can be concluded that the greatest negative area favored for electrophilic reaction is shown by the red color, while the most extreme positive district favored for nucleophilic reaction is illustrated by the blue color. The increase in the potential can be ordered as follow: blue > green > red, where blue demonstrates the powerful attraction while the red illustrates the powerful repulsion. Areas with negative values are distributed on nitrogen and sulfur atoms while the regions having the positive values are distributed on the hydrogen atoms.

3.5.6. Polarizability and Hyperpolarizability

DFT hypothesis has been utilized as an effective strategy to examine the organic nonlinear optical materials. The associations of electromagnetic fields in different media to create another fields changed in phase, frequency, amplitude or other propagation characteristics from the incident field gives rise to NLO [34]. The polarizability and hyperpolarizability describe the reaction of a framework in any given electric field [35]. They could decide not just the quality of the strength of molecular communications (for example, the long-range induction, and dispersion forces), the cross-areas of various scattering and collision forms, additionally, the NLO of the framework [36]. The hypothesis of electric polarizability is a main component of the normal translation of an extensive variety of phenomena, from nonlinear optics and electron scattering [37] to ones initiated by intermolecular collaborations..

$$E = E° - \mu_\alpha F_\alpha - 1/2\alpha_{\alpha\beta}F_\alpha F_\beta - 1/6\beta_{\alpha\beta\gamma}F_\alpha F_\beta F_\gamma + \ldots$$

Where E° is the energy of unperturbed molecule, F_α the field at the starting point, μ_α, $\alpha_{\alpha\beta}$ and $\beta_{\alpha\beta\gamma}$ are the components of dipole moment, polarizability and the first order hyperpolarizabilities, respectively. The total dipole moment (μ), the mean diole polarizability (α), the anisotropy of the polarizability (Δα) and the total first order hyperpolarizability β_{total}, utilizing x, y, z components they are defined as

$$\mu = (\mu_x^2 + \mu_y^2 + \mu_z^2)^{1/2}$$

$$\langle\alpha\rangle = \frac{\alpha_{xx} + \alpha_{yy} + \alpha_{zz}}{3}$$

$$\Delta\alpha = 2^{-1/2}\left[(\alpha_{xx} - \alpha_{yy})^2 + (\alpha_{yy} - \alpha_{zz})^2 + (\alpha_{zz} - \alpha_{xx})^2 + 6\alpha_{xx}^2\right]^{1/2}$$

$$\beta_{total} = (\beta_x^2 + \beta_y^2 + \beta_z^2)^{1/2}$$

And

$$\beta_x = \beta_{xxx} + \beta_{xyy} + \beta_{xzz}$$

$$\beta_y = \beta_{yyy} + \beta_{xxy} + \beta_{yzz}$$

$$\beta_z = \beta_{zzz} + \beta_{xxz} + \beta_{yyz}$$

In the recent study, the estimated dipole moment, polarizability and first order hyperpolarizability values are calculated and listed in Table 5.

3.5.7. Mulliken atomic charges

Mulliken atomic charge computation has a noteworthy part in the use of quantum concoction estimation to molecular framework on account of atomic charges impact, electronic structure, molecular polarizability, dipole moment and other properties of the framework. The estimated values of H_2PhT are recorded in Table 6. Figure 8 illustrates the charge distribution structure of H_2PhT. The S(8) and N(7) atoms revealed a negative charge because of their donating property. Moreover, S(8) atom has bigger ones more than N(7) atoms. Hydrogen atoms display positive charges because of its accepting property. Figure 13 illustrates the atoms numbering of H_2PhT.

3.6. DNA-methyl green bioassay

All prepared compounds were evaluated in the DNA methylgreen assay (Fig. 14). H_2PhT ligand and $[Pd(HPhT)_2]$ complex exhibited the most potent activity as a DNA interacting agent, with an IC_{50} value of 34.5 and 39.8 µg/ml, respectively, while $[Pt(H_2PhT)Cl_2]$ and $[Pt(H_2PhT)_2Cl_2]$ complexes showed moderate DNA interacting properties with IC_{50} value of 47.1 and 61.3 µg/ml, respectively. $[Cu(HPhT)(H_2O)Cl]$ complex exhibited the lowest DNA interacting activity.

3.7. Antimicrobial and Antimycotic Activities in terms of MIC (µg/mL).

All the isolated compounds were assayed *in vitro* against *E. coli* ATCC 25922, *S. aureus* ATCC 25923 for the determination of antibacterial activity. *C. albicans* ATCC 10231 was utilized for the assurance of antifungal behavior. Ciprofloxacin and fluconazole were utilized as reference medications in order to compare the antimicrobial activity. As found in Table 7, the H_2PhT and its chelates demonstrated diverse action against standard Gram-negative microbes "*E. coli, P*", H_2PhT has the highest antibacterial activity with MIC value of 4.68 followed by $[Pd(HPhT)_2]$ complex. H_2PhT and its $[Pd(HPhT)_2]$ complex demonstrated interesting behavior against the tested Gram-negative strains "*S. aureus*". H_2PhT showed higher antibacterial activity against ***S. aureus*** with MIC value equals 3.12 µg/ml related to the control medication. Table 7 demonstrated that all compounds introduced diverse MICs against *C. albicans* contrasted with the control fluconazole (1.17 µg/ml). Both H_2PhT and $[Pd(HPhT)_2]$ showed the highest antifungal activity against *C. Albicans* as compared with fluconazole. $[Cu(HPhT)(H_2O)Cl]$ complex showed the lowest antibacterial and antiviral activities among the prepared compounds.

4. Conclusion

Divalent platinum, palladium and copper chelates of H_2PhT have been isolated by the reaction of 2-aminobenzothiazole and phenyl isothiocyanate. The ligand H_2PhT behaves as monobasic bi-dentate in Cu(II) and Pd(II) chelates while it behaves as neutral bi-dentate in both Pt(II) complexes. The spectral analysis reveals a tetrahedral coordination geometry for $[Cu(HPhT)(H_2O)Cl]$, a square planar geometry for both $[Pd(HPhT)_2]$ and $[Pt(H_2PhT)_2Cl_2]$ and octahedral geometry for $[Pt(H_2PhT)_2Cl_2]$. The solid IR confirmed the presence of the ligand in the thione form while ^1H- and ^{13}C-NMR spectra suggested the presence of H_2PhT in the thiol form in solution. The molecular modeling are drawn and indicated chemical reactivity, MEP, NLO, Mulliken atomic charges, and total energy for all the isolated compounds. Theoretical infrared intensities and ^1H NMR of H_2PhT was calculated using DFT method. An examination of the exploratory and hypothetical spectra can be extremely helpful in making right assignments and comprehension the fundamental synthetic chemical shift. The DNA bioassay, antibacterial and antifungal activities of the prepared compounds have been screened. The H_2PhT and $[Pd(HPhT)_2]$ exhibited the most potent activity as a DNA interacting agent. In addition, H_2PhT has the highest antibacterial activity followed by $[Pd(HPhT)_2]$.

References:

[1] S. Cronje, H.G. Raubenheimer, H.S. Spies, C. Esterhuysen, H. Schmidbaur, A. Schier, G.J. Kruger, Synthesis and characterisation of N-coordinated pentafluorophenyl gold (I) thiazole-derived complexes and an unusual self-assembly to form a tetrameric gold (I) complex, Dalton Transactions, (2003) 2859-2866.

[2] W.M. Singh, J.B. Baruah, Nickel, copper and zinc complexes of (2-methoxycarbonylmethylimino-5-methyl-thiazol-3-yl)-acetic acid, Polyhedron, 27 (2008) 2968-2972.

[3] F. Téllez, A. Peña-Hueso, N. Barba-Behrens, R. Contreras, A. Flores-Parra, Coordination compounds in a pentacyclic aromatic system from 2-aminobenzothiazole derivatives and transition metal ions, Polyhedron, 25 (2006) 2363-2374.

[4] M. Conte, J. Lafon, T. Avignon, J. Metzger, Application des champs de forces du thiazole et du benzene aux monophényl-thiazoles. utilisationàla détermination des angles dièdres, Journal of Molecular Structure, 30 (1976) 169-180.

[5] A.I. Vogel, Vogel's textbook of quantitative chemical analysis, Fifth ed., Longmans, London, 1989.

[6] A.D. Becke, Density-functional thermochemistry. III. The role of exact exchange, The Journal of chemical physics, 98 (1993) 5648-5652.

[7] C. Lee, W. Yang, R.G. Parr, Development of the Colle-Salvetti correlation-energy formula into a functional of the electron density, Physical review B, 37 (1988) 785.

[8] P. Sharma, A. Gupta, K. Rao, F.J. Owens, R. Sharma, R. Ahuja, J.O. Guillen, B. Johansson, G. Gehring, Ferromagnetism above room temperature in bulk and transparent thin films of Mn-doped ZnO, Nature materials, 2 (2003) 673-677.

[9] R. Ditchfield, Molecular orbital theory of magnetic shielding and magnetic susceptibility, The Journal of Chemical Physics, 56 (1972) 5688-5691.

[10] K. Wolinski, J.F. Hinton, P. Pulay, Efficient implementation of the gauge-independent atomic orbital method for NMR chemical shift calculations, Journal of the American Chemical Society, 112 (1990) 8251-8260.

[11] M. Frisch, G. Trucks, H. Schlegel, G. Scuseria, M. Robb, J. Cheeseman, G. Scalmani, V. Barone, B. Mennucci, G. Petersson, Gaussian 09, Revision A. 02; Gaussian, Inc: Wallingford, CT, 2009, There is no corresponding record for this reference, (2015).

[12] A.M. Zaghloul, A.A. Gohar, Z.A.-A.M. Naiem, F.M.A. Bar, Taxodione, a DNA-binding compound from Taxodium distichum L.(Rich.), Zeitschrift für Naturforschung C, 63 (2008) 355-360.

[13] N.S. Burres, A. Frigo, R.R. Rasmussen, J.B. McAlpine, A Colorimetric Microassay for the Detection of Agents that Interact with DNA, Journal of Natural Products, 55 (1992) 1582-1587.

[14] C.R. Prakash, S. Raja, Synthesis, characterization and in vitro antimicrobial activity of some novel 5-substituted Schiff and Mannich base of isatin derivatives, Journal of Saudi Chemical Society, 17 (2013) 337-344.

[15] W.J. Geary, The use of conductivity measurements in organic solvents for the characterisation of coordination compounds, Coordination Chemistry Reviews, 7 (1971) 81-122.

[16] S.S. Kandil, N.H.M. Yarkandi, S.M.S. Jambi, Coordination of cobalt(III), nickel(II), copper(II), palladium(II) and platinum(II) with N-ethyl-N′-(4′-methylthiazol-2′-yl)thiourea (HL), Journal of Sulfur Chemistry, 35 (2014) 98-105.

[17] S.S. Kandil, S.M. Katib, N.H. Yarkandi, Nickel (II), palladium (II) and platinum (II) complexes of N-allyl-N′-pyrimidin-2-ylthiourea, Transition Metal Chemistry, 32 (2007) 791-798.

[18] R.J. Corriu, E. Lancelle-Beltran, A. Mehdi, C. Reyé, S. Brandès, R. Guilard, Hybrid materials containing metal (II) Schiff base complex covalently linked to the silica matrix by two Si-C bonds: Reaction with dioxygen, Chemistry of materials, 15 (2003) 3152-3160.

[19] J. Ribas, C. Diaz, R. Costa, Y. Journaux, C. Mathoniere, O. Kahn, A. Gleizes, Structure and magnetic and spectroscopic properties of a nickelIIcopperIInickelII trinuclear species, Inorganic Chemistry, 29 (1990) 2042-2047.

[20] A. Lever, The electronic spectra of tetragonal metal complexes analysis and significance, Coordination Chemistry Reviews, 3 (1968) 119-140.

[21] O. El-Gammal, G.A. El-Reash, S. Ghazy, A. Radwan, Synthesis, characterization, molecular modeling and antioxidant activity of (1E, 5E)-1, 5-bis (1-(pyridin-2-yl) ethylidene) carbonohydrazide (H 2 APC) and its zinc (II), cadmium (II) and mercury (II) complexes, Journal of Molecular Structure, 1020 (2012) 6-15.

[22] G.A. El-Reash, O. El-Gammal, S. Ghazy, A. Radwan, Characterization and biological studies on Co (II), Ni (II) and Cu (II) complexes of carbohydrazones ending by pyridyl ring, Spectrochimica Acta Part A: Molecular and Biomolecular Spectroscopy, 104 (2013) 26-34.

[23] G.A. El-Reash, O. El-Gammal, A. Radwan, Molecular structure and biological studies on Cr (III), Mn (II) and Fe (III) complexes of heterocyclic carbohydrazone ligand, Spectrochimica Acta Part A: Molecular and Biomolecular Spectroscopy, 121 (2014) 259-267.

[24] O. El-Gammal, T. Rakha, H. Metwally, G.A. El-Reash, Synthesis, characterization, DFT and biological studies of isatinpicolinohydrazone and its Zn (II), Cd (II) and Hg (II) complexes, Spectrochimica Acta Part A: Molecular and Biomolecular Spectroscopy, 127 (2014) 144-156.

[25] W. Linert, A. Taha, Co-ordination of solvent molecules to square-planar mixed-ligand nickel (II) complexes: a thermodynamic and quantum-mechanical study, Journal of the Chemical Society, Dalton Transactions, (1994) 1091-1095.

[26] R. Dennington, T. Keith, J. Millam, Semichem Inc, Shawnee Mission KS, GaussView, Version, 5 (2009).

[27] R.G. Parr, R.G. Pearson, Absolute hardness: companion parameter to absolute electronegativity, Journal of the American Chemical Society, 105 (1983) 7512-7516.

[28] R.G. Parr, L.v. Szentpaly, S. Liu, Electrophilicity index, Journal of the American Chemical Society, 121 (1999) 1922-1924.

[29] M. Govindarajan, M. Karabacak, S. Periandy, D. Tanuja, Spectroscopic (FT-IR, FT-Raman, UV and NMR) investigation and NLO, HOMO–LUMO, NBO analysis of organic 2, 4, 5-trichloroaniline, Spectrochimica Acta Part A: Molecular and Biomolecular Spectroscopy, 97 (2012) 231-245.

[30] E. Scrocco, J. Tomasi, Electronic Molecular Structure, Reactivity and Intermolecular Forces: An Euristic Interpretation by Means of Electrostatic Molecular Potentials, in: L. Per-Olov (Ed.) Advances in Quantum Chemistry, Academic Press, 1978, pp. 115-193.

[31] F.J. Luque, J.M. López, M. Orozco, Perspective on "Electrostatic interactions of a solute with a continuum. A direct utilization of ab initio molecular potentials for the prevision of solvent effects", in: Theoretical Chemistry Accounts, Springer, 2000, pp. 343-345.

[32] N. Okulik, A.H. Jubert, Theoretical analysis of the reactive sites of non-steroidal anti-inflammatory drugs, Internet Electron. J. Mol. Des, 4 (2005) 17-30.

[33] P. Politzer, P.R. Laurence, K. Jayasuriya, Molecular electrostatic potentials: an effective tool for the elucidation of biochemical phenomena, Environmental health perspectives, 61 (1985) 191.

[34] Y.-X. Sun, Q.-L. Hao, W.-X. Wei, Z.-X. Yu, L.-D. Lu, X. Wang, Y.-S. Wang, Experimental and density functional studies on 4-(3, 4-dihydroxybenzylideneamino) antipyrine, and 4-(2, 3, 4-trihydroxybenzylideneamino) antipyrine, Journal of Molecular Structure: THEOCHEM, 904 (2009) 74-82.

[35] Q.-q. Zhang, S. Lei, X. Wang, L. Wang, P. Yu, Y. Chen, X. Zeng, L. Chen, W. Zhao, J. Zu, Research on discrimination of 3D fluorescence spectra of phytoplanktons, Spectroscopy and Spectral Analysis, 24 (2004) 1227-1229.

[36] O. Christiansen, J. Gauss, J.F. Stanton, Frequency-dependent polarizabilities and first hyperpolarizabilities of CO and H 2 O from coupled cluster calculations, Chemical physics letters, 305 (1999) 147-155.

[37] N. Lane, The theory of electron-molecule collisions, Reviews of Modern Physics, 52 (1980) 29.

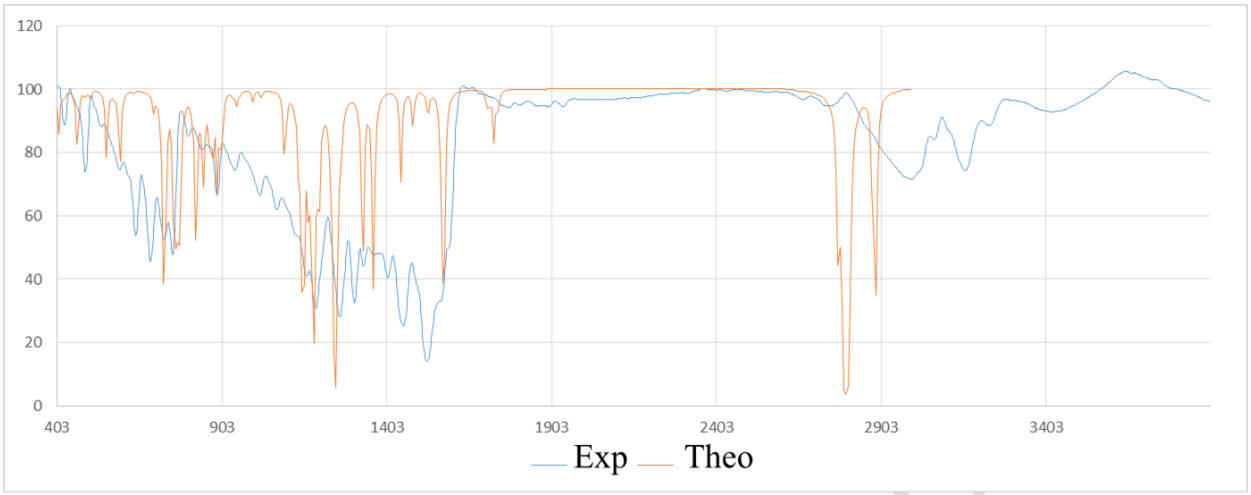

Fig. 1. Comparison of experimental and theoretical IR spectra of H_2PhT.

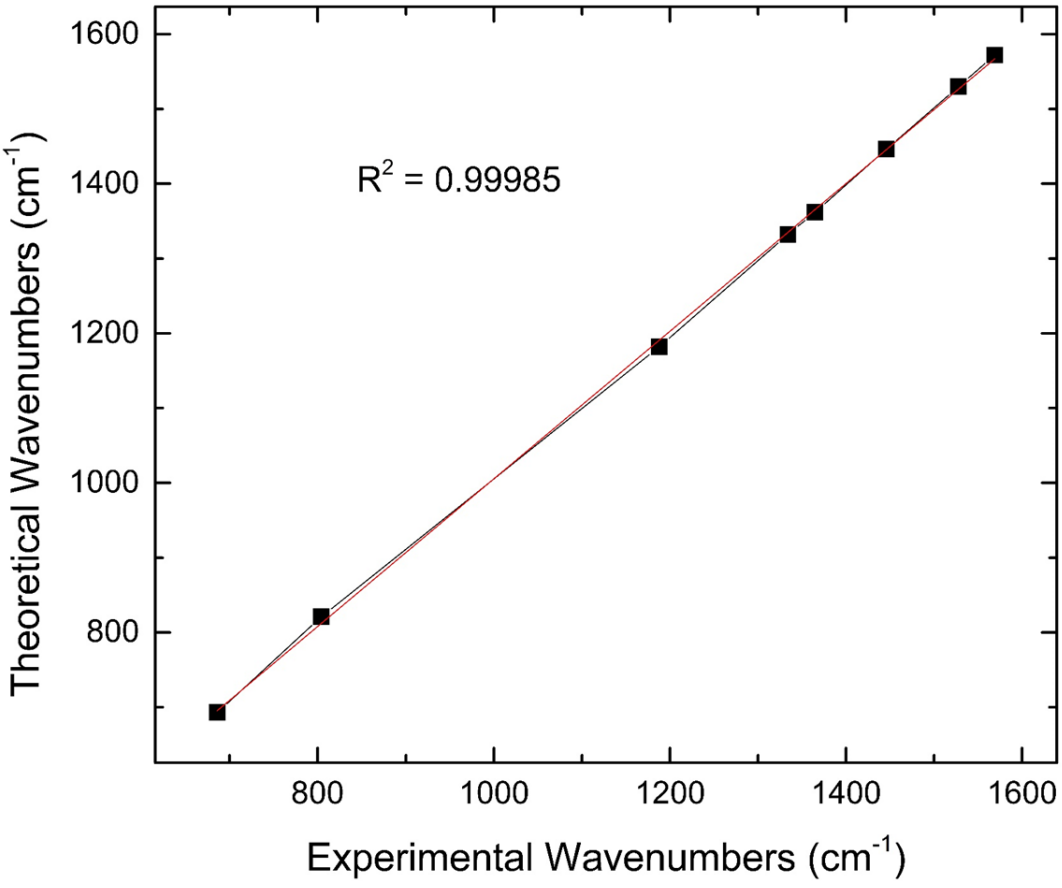

Fig. 2. The linear regression between the experimental and theoretical (keto form) frequencies of H_2PhT.

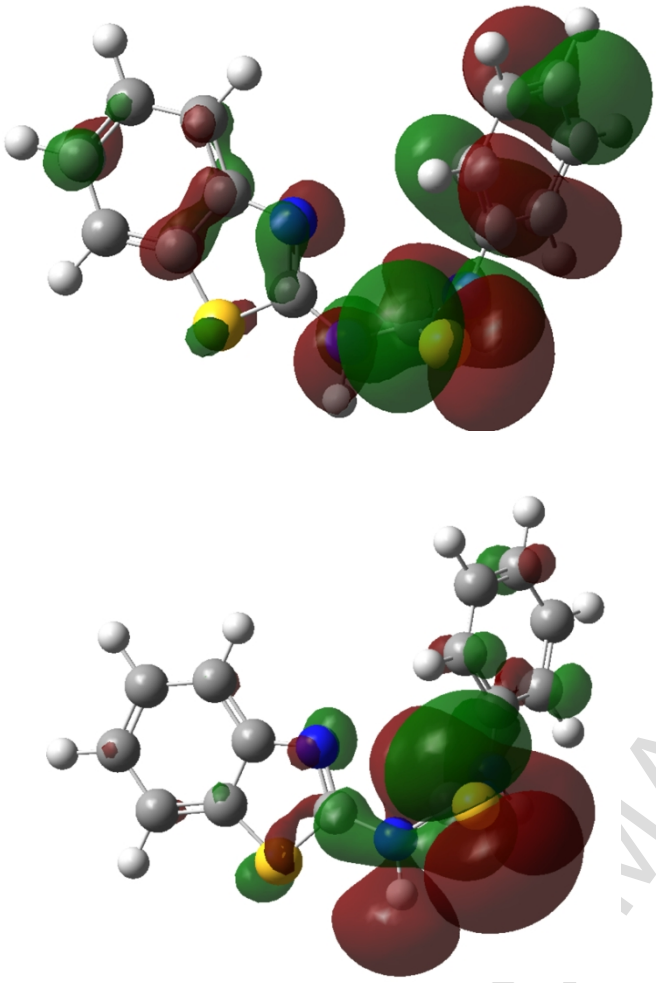

E_{LUMO}= -2.79eV

(excited state)

$E_{HOMO=}$ -5.15 eV

(ground state)

Fig. 3. 3D plots frontier orbital energies using DFT method for H_2PhT.

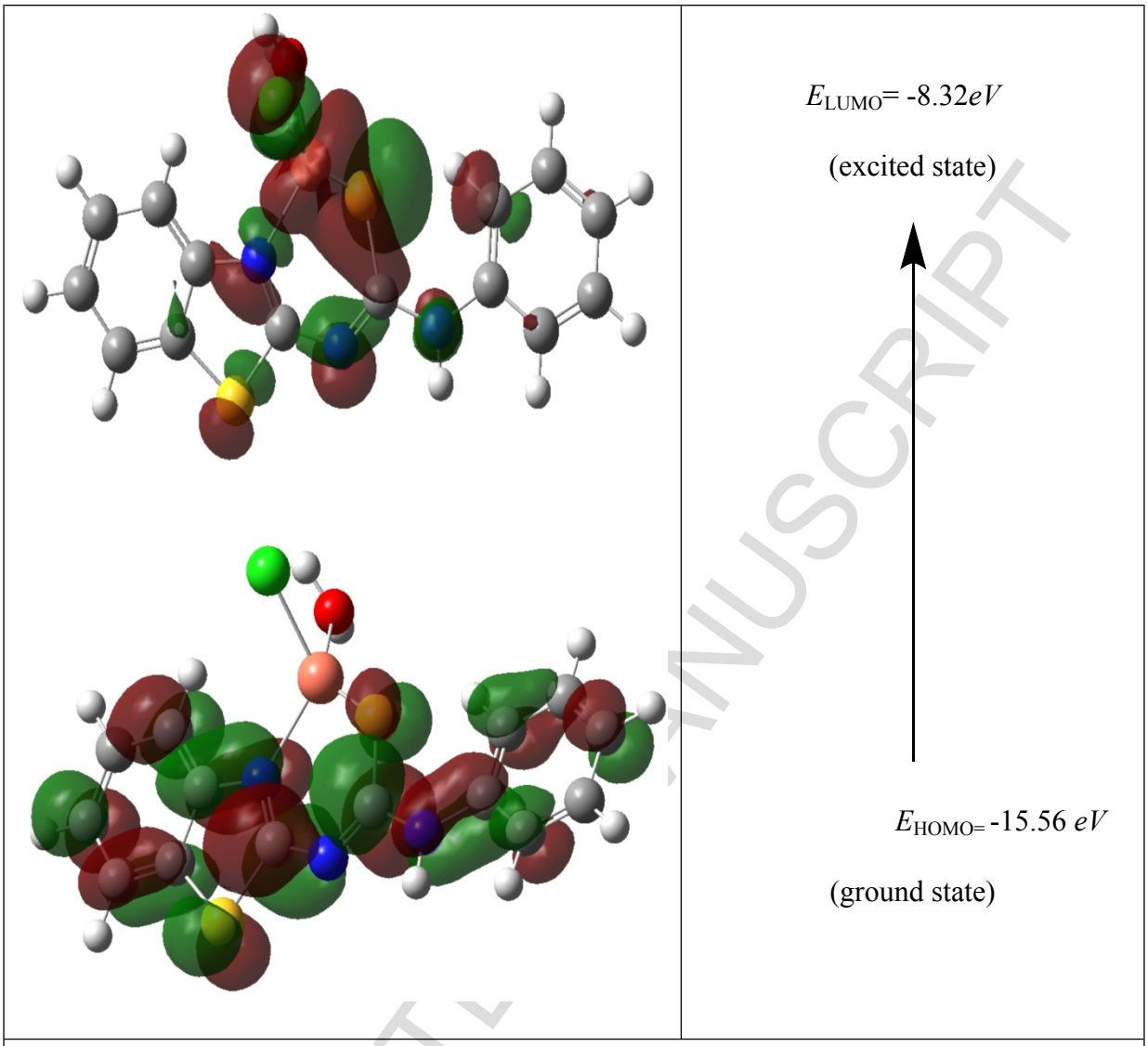

Fig. 4. 3D plots frontier orbital energies using DFT method for [Cu(HPhT)(H_2O)Cl].

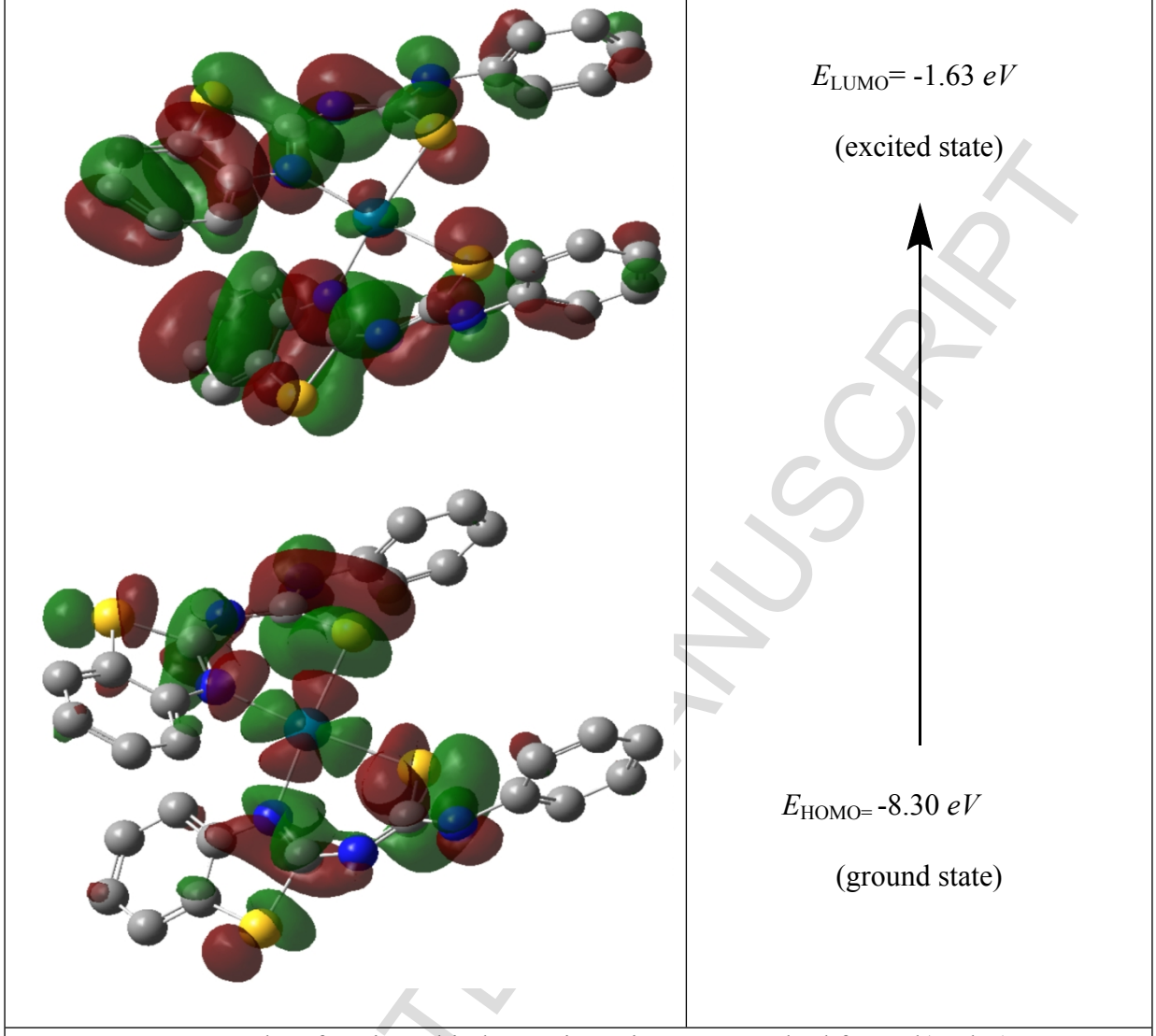

Fig. 5. 3D plots frontier orbital energies using DFT method for [Pd(HPhT)$_2$].

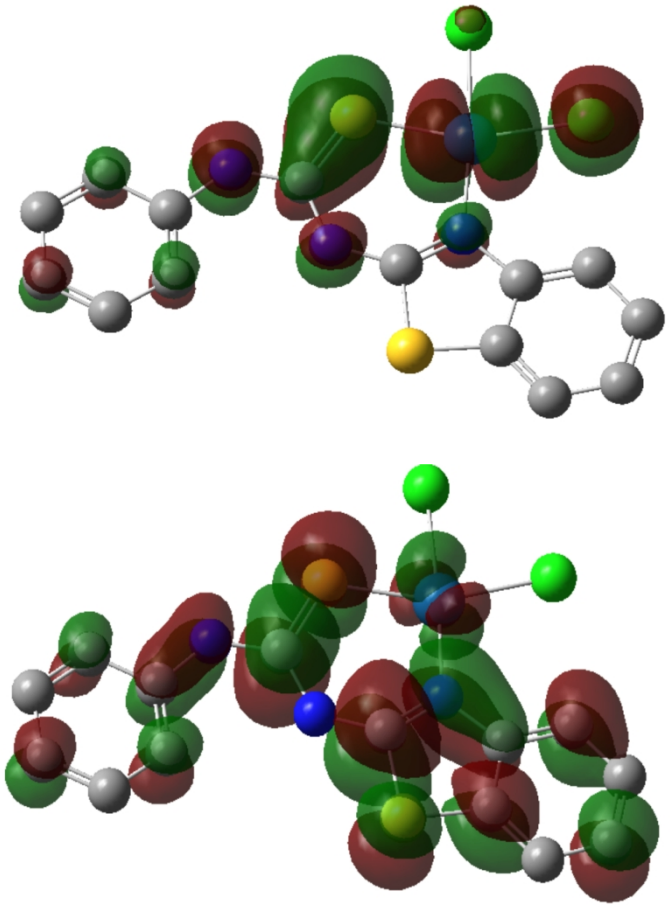

E_{LUMO}= -2.21 *eV*

(excited state)

E_{HOMO}= -8.40 *eV*

(ground state)

Fig. 6. 3D plots frontier orbital energies using DFT method for [Pt(H_2PhT)Cl_2].

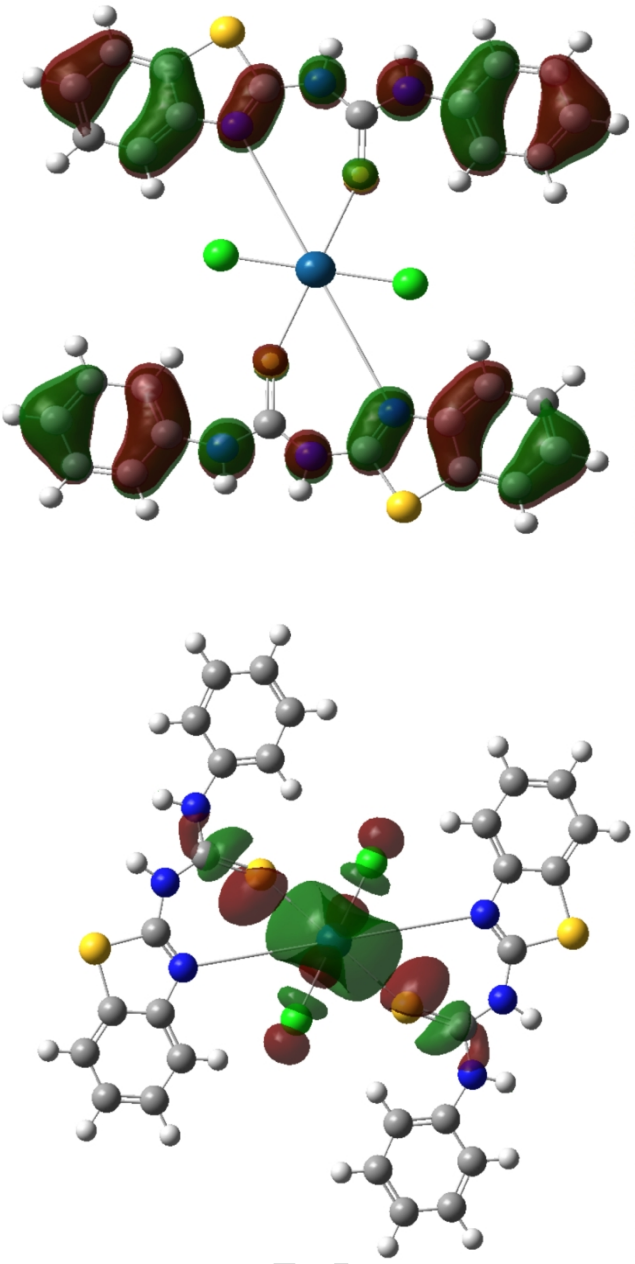

E_{LUMO}= -0.056eV

(excited state)

E_{HOMO}= -8.63 eV

(ground state)

Fig. 7. 3D plots frontier orbital energies using DFT method for [Pt(H_2PhT)$_2$$Cl_2$].

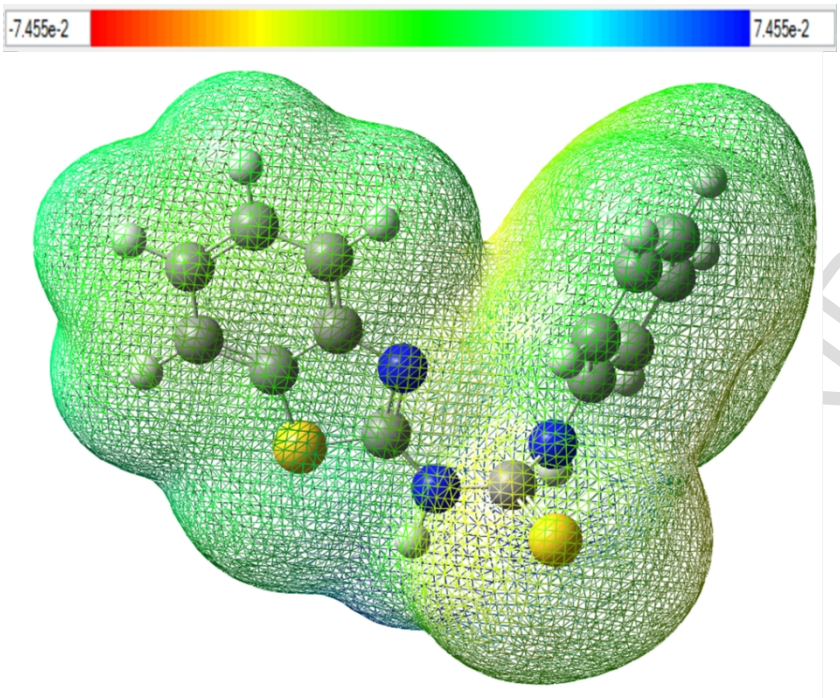

Fig. 8. Molecular electrostatic potential map for H_2PhT.

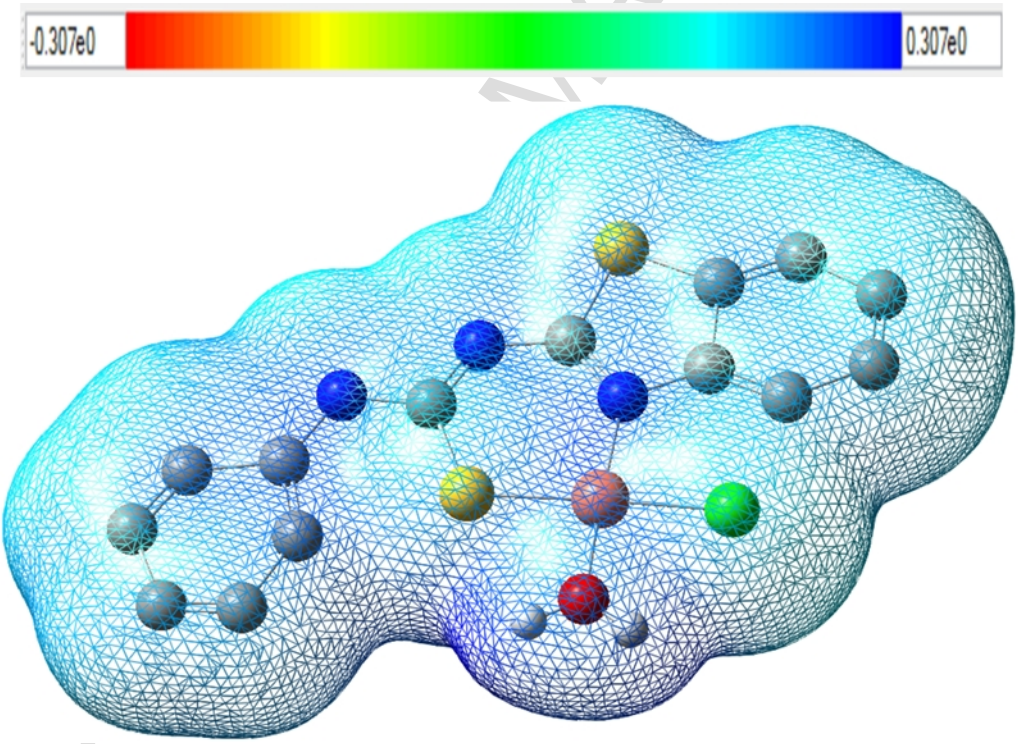

Fig. 9. Molecular electrostatic potential map for [Cu(HPhT)(H_2O)Cl].

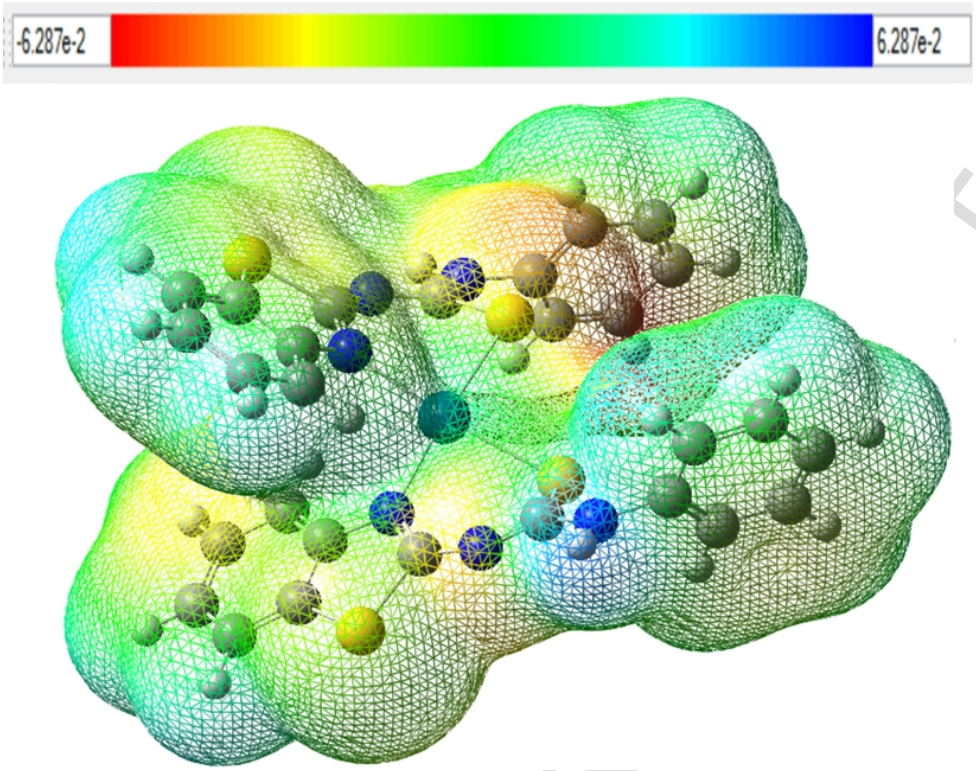

Fig. 10. Molecular electrostatic potential map for [Pd(HPhT)$_2$].

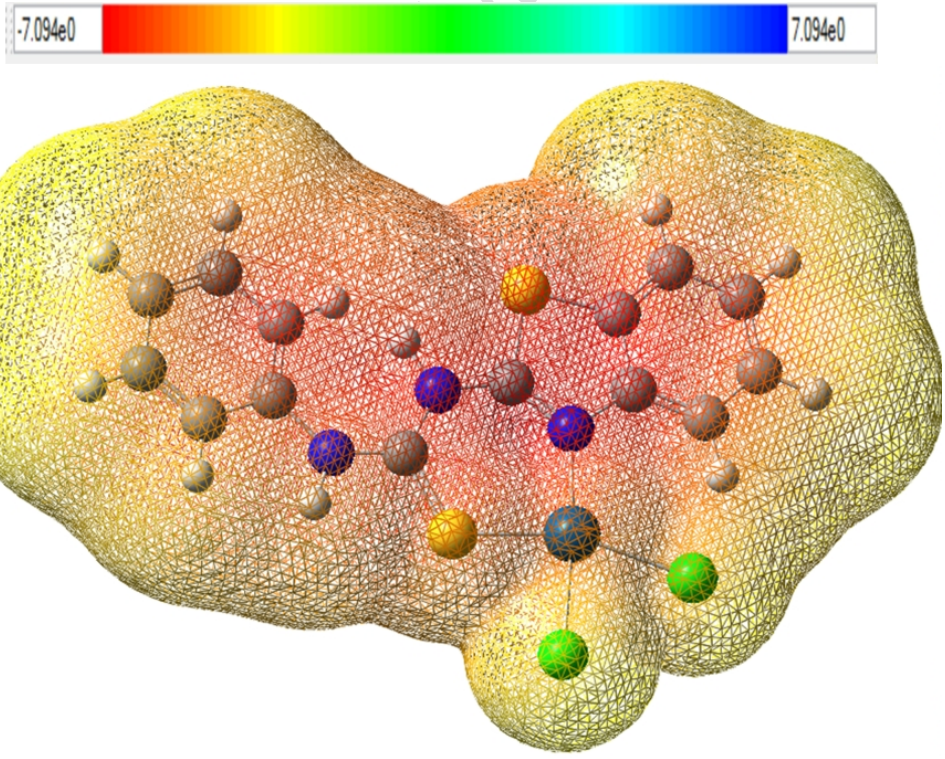

Fig. 11. Molecular electrostatic potential map for [Pt(H_2PhT)Cl_2].

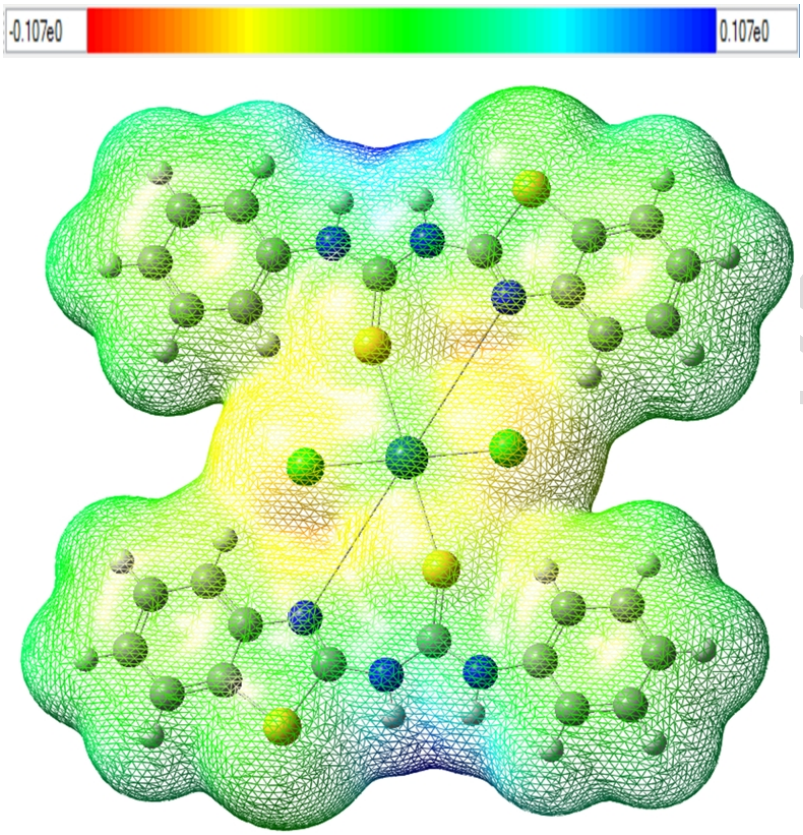

Fig. 12. Molecular electrostatic potential map for $[Pt(H_2PhT)_2Cl_2]$.

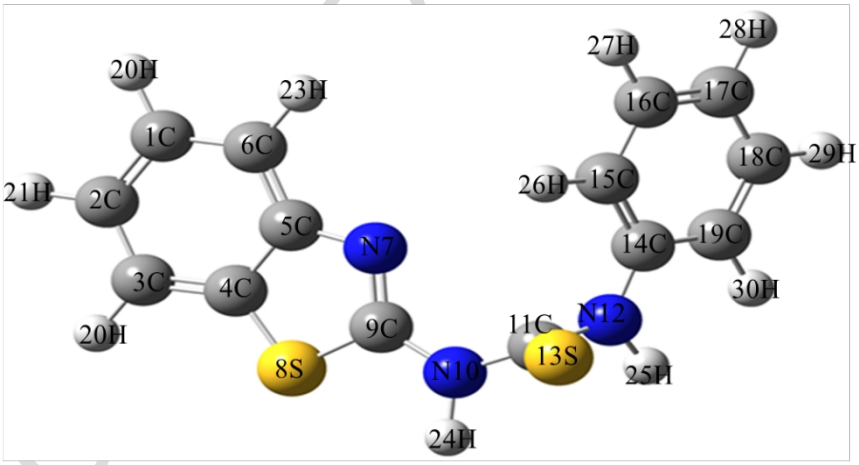

Fig. 13. The Mulliken charge distribution for H_2PhT.

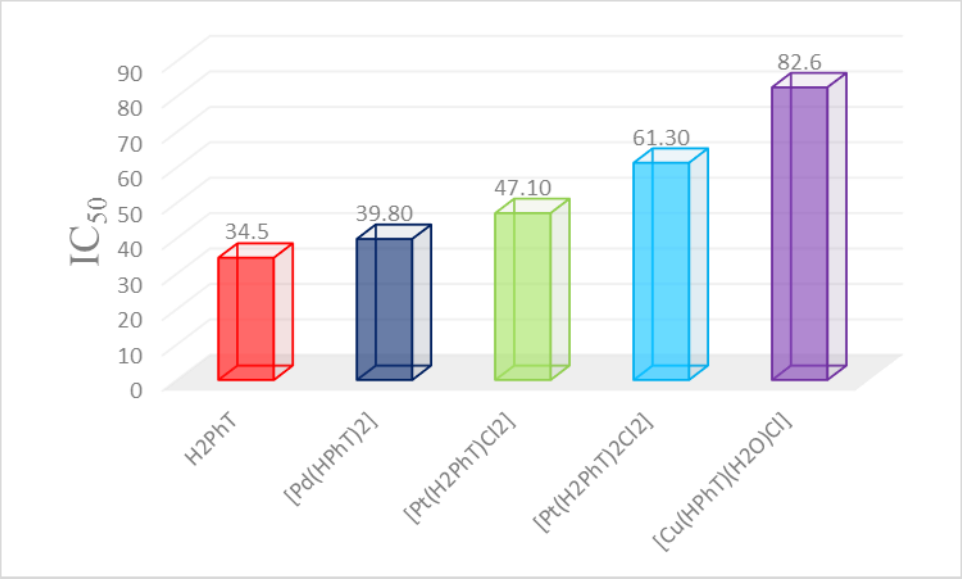

Fig. 14. DNA/methyl green colourimetric assay of the DNA-binding compounds (IC_{50} values represent the concentration (mean ± SD, n = 3-5 separate determinations) required for a 50% decrease in the initial absorbance of the DNA/methyl green solution).

Table 1. Analytical and physical data of H_2PhT and its Cu(II), Pd(II) and Pt(II) complexes.

Compound			% Found (Calcd.)					Yield
Empirical formula,		Colour						(%)
	(F.Wt)		M	Cl	C	H	N	
(H_2PhT) $C_{14}H_{11}N_3S_2$	(285.38)	Pale yellow	-	-	58.92 (58.02)	3.89 (3.52)	14.72 (14.64)	85
$[Cu(HPh)_2(H_2O)Cl]$		Olive green	15.80	8.80	42.89	2.50	11.37	80
$C_{14}H_{12}CuN_3OS_2$	(401.39)		(15.83)	(8.83)	(43.13)	(2.39)	(11.42)	
$[Pd(HPhT)_2]$		Reddish-brown	15.70	-	48.40	1.89	12.05	87
$C_{28}H_{20}N_6PdS_4$	(675.17)		(15.76)	-	(48.56)	(1.75)	(11.90)	
$[Pt(H_2PhT)Cl_2]$		Yellow	35.32	12.78	31.59	1.45	8.27	88
$C_{14}H_{11}Cl_2PtN_3S_2$	(551.37)		(35.38)	(12.86)	(31.50)	(1.39)	(8.19)	
$[Pt(H_2PhT)_2Cl_2]$		Yellow	23.26	8.42	40.19	2.05	10.04	82
$C_{28}H_{22}Cl_2PtN_6S_4$	(836.75)		(23.31)	(8.47)	(40.22)	(1.97)	(10.37)	

Table 2. Assignments of IR spectral bands of H_2PhT and its Cu(II), Pd(II) and Pt(II) complexes.

			Thiazole ring vib.		
Compound	υ(N1–H)	υ(N2–H)	ν(C=C) + ν(C=N)	$\nu(C\text{-}S\text{-}C)_{thiazole}$	$\nu(CS)_{thiourea}$
H_2PhT	3436	3162	1569, 1528	686	804
$[Cu(HPhT)(H_2O)Cl]$	-	3124	1598, 1535	686	747
$[Pd(HPhT)_2]$	-	3116	1591, 1529	684	787
$[Pt(H_2PhT)_2Cl_2]$	3457	3124	1594, 1538	690	790
$[Pt(H_2PhT)_2Cl_2]$	3461	3108	1594, 1533	687	792

Table 3. The ^{1}H NMR chemical shifts (ppm) of H_2PhT ligand.

Method	Chemical shift (ppm)
TMS B3LYP/6-311+G(2d,p) GIAO Correlation analysis (Experimental)	10.71(10.46), 6.50, 6.15, 6.02, 5.94, 5.82, 5.37, 4.96(7.28-7.95), 1.38(1.92).

Table 4. Calculated E_{HOMO}, E_{LUMO}, energy band gap ($E_{HOMO} - E_{LUMO}$), dipole moment (DM) chemical potential (μ), electronegativity (χ), global hardness (η), global softness (σ), global electrophilicity index (ω) and total energy (TE) for H_2PhT and its complexes.

	E_{HOMO} (a.u.)	E_{LUMO} (a.u.)	ΔE (a.u.)	DM (D)	η (a.u.)	σ (a.u.)$^{-1}$	μ (a.u.)	χ(a.u.)	ω (a.u)	TE (a.u.)
H_2PhT	-0.20251	-0.10251	0.30502	3.9943	0.05	20	-0.15251	0.15251	0.232593	-1500.3
[Cu(HPhT)(H_2O)Cl]	-0.57193	-0.30572	0.87765	8.9997	0.133105	7.512866	-0.43883	0.438825	0.723366	-3661.39
[Pd($HPhT)_2$]	-0.30514	0.06007	0.24507	1.5045	0.182605	5.476301	-0.12254	0.122535	0.041113	-7888.32
[Pt(H_2PhT)Cl_2]	-0.3089	0.08126	0.22764	14.7753	0.19508	5.126102	-0.11382	0.11382	0.033204	0.162432
[Pt($H_2PhT)_2$ Cl_2]	-0.31727	-0.00205	0.31932	0.0005	0.15761	6.344775	-0.15966	0.15966	0.080868	-1586.58

Table 5. The dipole moments μ (D), polarizability α, the average polarizability ‹α›, the anisotropy of the polarizability Δα and the first order hyperpolarizability β of H_2PhT ligand.

Parameter of H_2PhT			
β_{xxx}	-333.92	μ_y	-0.1305
β_{xxy}	-105.56	μ_z	-1.3089
β_{xyy}	-166.29	μ(D)	1.5714
β_{yyy}	-22.78	αxx	2.51E+02
β_{zxx}	647.76	αxy	-1.3063898
β_{xyz}	483.15	αyy	2.53E+02
β_{zyy}	210.33	αxz	6.88E+00
β_{xzz}	-111.93	αyz	2.81E-01
β_{yzz}	-31.599	αzz	1.37E+02
β_{zzz}	184.16	‹α› (e.s.u)	31.714E-24
β_{tot} (e.s.u)	10.453E-30	Δα (e.s.u)	66.718E-24
μ_x	-0.8597		

Table 6. The Mulliken charge distribution for H_2PhT.

Atoms	Mulliken charges	Atoms	Mulliken charges	Atoms	Mulliken charges
C1	-0.466	C11	-0.328	H21	0.188
C2	-0.515	N12	-0.108	H22	0.204
C3	-0.697	S13	0.185	H23	0.227
C4	1.011	C14	-1.064	H24	0.463
C5	0.623	C15	1.520	H25	0.398
C6	-0.936	C16	-0.906	H26	0.223
N7	-0.018	C17	0.079	H27	0.193
S8	-0.071	C18	-0.333	H28	0.185
C9	-0.368	C19	-0.379	H29	0.188
N10	0.137	H20	0.1907	H30	0.174

Table 7. Antimicrobial activity as MICs (**µ**g/ml) of the prepared compounds and the references drugs.

	MICs (µg/ml)		
Compound	***E. coli***	***S. aureus***	***C. Albicans***
H_2PhT	4.68	3.12	1.56
$[Pt(H_2PhT)Cl_2]$	18.75	9.37	4.68
$[Pd(HPhT)_2]$	9.37	4.68	2.34
$[Pt(H_2PhT)_2Cl_2]$	37.5	25	12.5
$[Cu(HPhT)(H_2O)Cl]$	75	50	37.5
Ciprofloxacin	1.56	0.78	----
Fluconazole	----	----	1.17